Resonance Raman spectroscopy and ultrafast chemical dynamics

Nandita Biswas and Siva Umapathy

Department of Inorganic and Physical Chemistry, Indian Institute of Science, Bangalore 560 012, India

Resonance Raman (RR) spectroscopy is normally used to study the excited state structure and dynamics of various photochemical and photophysical processes. In this article, we briefly discuss the various applications of RR spectroscopy and show how experimental RR intensities along with time-dependent wavepacket dynamical calculations can be used to study the excited state structure and ultrafast dynamics (~ 10^{-15} secs).

1. Introduction

With the availability of tunable lasers, resonance Raman (RR) spectroscopy has become a widely-used technique to probe the structure and dynamics of short-lived excited state intermediates of various photochemical and photophysical processes[1–14]. Although electronic spectroscopy is also useful in providing information about lifetime and decay rates of the excited states of polyatomic molecules, it often lacks vibrational mode-specific information due to its unresolved and unstructured envelope, in the condensed phase, at room temperature (RT). Thus, in order to extract valuable excited state structural information present in the molecule, RR spectroscopic technique is normally used.

Under pre-resonance or resonance conditions, i.e. when the excitation energy approaches or coincides with a particular electronic transition of the system under investigation, the RR spectra show enormous intensity enhancement which contain information about the excited state potential energy surface and hence, in turn can dictate the initial dynamics of nuclear motion in the Franck–Condon (FC) region. Such dynamical processes can be intuitively understood through time-dependent quantum (wavepacket) dynamics. Figure 1 illustrates harmonic ground (S_0) as well as excited (S_1) potential energy surfaces along a normal coordinate, where S_1 is displaced relative to S_0 by an amount Δ. In the figure it is shown that using different excitation energies, viz. E_1, E_2 and E_3 (where, $E_1 > E_2 > E_3$) we can probe various regions of the Franck–Condon potential energy surface. Thus, the region of maximum FC overlap (marked b in the figure) represents the maximum of the absorption band and the region marked a and c represent the region of moderate FC overlap and hence, moderate absorption in the electronic absorption spectrum. Since the resonance Raman intensities are governed by the FC factors (*vide infra*), an analysis of the observed Raman intensities of each vibrational mode for different excitation wavelengths can provide mode-dependent dynamical information. Therefore, the distortions that the molecule undergoes following photoexcitation from ground to resonant excited electronic state, within the electronic dephasing time scale can easily be monitored using this technique.

Wavelength dependence of the Raman scattering intensity, viz. Raman excitation profiles (REPs) provide information on the origin of RR intensities and also the dynamics associated with the resonant excited state[1,7,9,15,16]. Qualitatively, if the vibrational modes are FC active in the resonant electronic state, then the Raman intensities are enhanced for these modes due to A-term Raman scattering[17–19]. Therefore, the REPs of these vibrational modes are expected to follow the absorption spectral profile of the electronic state to which the resonant excitation is carried out. The REPs thus, carry, the observed information about the excited state potential energy surface, in the FC region. The knowledge of $\delta\omega$ (using LO-ac-tensities are essential in order to pro-terization of the excited state perimental val-

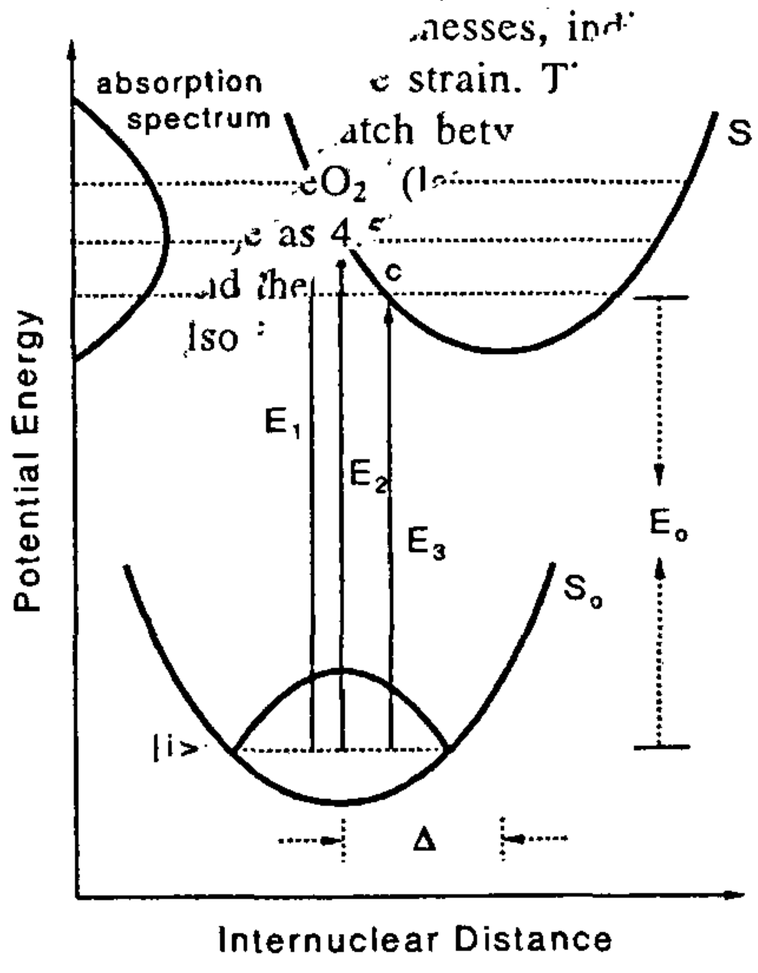

Figure 1. Schematic representation of Franck–Condon factors being a measure of the absorption cross section.

ultrafast dynamics and to know the extent of homogeneous and inhomogeneous broadening contributions.

The structural distortions in the excited electronic state can also be studied using time-resolved resonance Raman (TR^3) scattering[10–14] where a pump pulse is used to initiate the photochemical process. It is then followed by a probe pulse which is normally used to obtain the time-resolved resonance enhanced Raman spectrum of a transient intermediate. Thus, the conformational dynamics and decay kinetics of excited electronic states can be examined on the time scales of hundreds of femtoseconds to nano or milliseconds. Dynamics occurring in the range of tens of femtoseconds cannot be studied using this technique due to the limitation resulting from broad spectral band width of the laser pulse (dictated by the Uncertainty Principle). These processes can, therefore, be studied using RR intensity analyses which provide a means of probing the initial excited state dynamics of photochemically active systems.

In this review, we begin with §2, describing the experimental technique generally used to measure resonance Raman intensities. In §3, we present the theoretical and computational methods used to carry out RR intensity analyses with brief outline on the effect of resonance and pre-resonance interference, solvent perturbation, etc. Finally, in §4, we present applications of RR intensity analyses and we report our results obtained using the time-dependent quantum mechanical (TDQM) technique on the isomerization dynamics of *trans*-azobenzene and preliminary results on 4-dimethylamino, 4′-nitro-azobenzene in the excited electronic state. In order to man correlation of the use of RR spectroscopy in wavepacket along dynamics, we have reported mainly lose their phase and a few from the literature.

results

2. Experimen ods

Absolute Raman intensity rements are difficult but its knowledge is essential, since in relation to absorption cross section help in partition e total vibronic linewidths into homogeneous and mogeneous components[20–25]. The determination of abso Raman cross sections often depend on the availability o Raman intensity standards with known Raman cross sections for the excitation wavelength range of interest. The availability of commercial optical parametric oscillator (OPO) has enabled a simple method of determining the absolute Raman intensities utilizing the measurement of integrated intensity ratios[26].

The excitation wavelengths for the RR experiments in the visible region, viz. 440 to 600 nm were scanned using a tunable laser pulse output from an OPO (MOPO 730, Spectra Physics), pumped by a Nd–YAG laser (GCR 250, Spectra Physics) providing a high energy laser pulse of wavelength 355 nm. For the pre-resonance Raman experiments, the third harmonic output (355 nm) of a Spectra Physics DCR-11, Nd–YAG Q-switched laser, the first Stokes (416 nm) and second anti-Stokes (369 nm) hydrogen Raman shifted laser lines and the first Stokes methane Raman shifted laser line (396 nm) were used as excitation wavelengths. A SPEX 1404 double monochromator with two 600 groove gratings blazed at 500 nm was used to disperse the scattered light. A liquid nitrogen cooled charge coupled device (Princeton Instruments) with 576×378 pixels was used as the multichannel detector. The recorded Raman spectra were calibrated using known solvent bands as reference and the spectral resolution is estimated as 5 cm^{-1}. Depolarization ratios (ρ) of the Raman bands were determined by using a polarizer in combination with a scrambler. The solutions of *trans*-azobenzene in carbon tetrachloride (CCl_4) and 4-dimethyl amino, 4′-nitro-azobenzene in CCl_4 and benzonitrile (C_6H_5CN) were circulated through a capillary at the rate of about 10 ml/min to avoid photo-isomerization or local heating during exposure. The re-absorption of the resonance Raman scattered light by the sample was minimized by using a 180° backscattering collection geometry. The sample concentrations used for Raman experiments were about 5×10^{-2} M for *trans*-azobenzene and 1×10^{-3} M for 4-dimethylamino, 4′-nitro-azobenzene. The relative Raman intensities were obtained after normalization of the spectra with a solvent band[27,28] (CCl_4 doublet at 761 and 792 cm^{-1} or, C_6H_5CN band at 1000 cm^{-1}).

3. Theory of resonance Raman scattering intensities

3.1. Sum over states method

In the sum over states method, the resonance Raman amplitude in the energy frame, for the transition from the initial state $|i\rangle$ to the final state $|f\rangle$ (where $|i\rangle$ and $|f\rangle$ correspond to the initial and final vibrational eigenstates of the electronic ground state) in an isolated polyatomic molecule under the Born–Oppenheimer approximation, can be described by the Kramers–Heisenberg–Dirac (KHD) dispersion expression[29,30].

$$\alpha_{i\to f}(E_L) = M^2 \sum_v \frac{\langle f|v\rangle\langle v|i\rangle}{E_v - E_i + E_o - E_L - i\Gamma}, \qquad (1)$$

where, E_o is the energy separation between the zeroth vibrational levels of the ground and the excited electronic states, E_v the energy corresponding to the vibrational state $|v\rangle$ of the excited electronic state and E_i the zero-point vibrational energy of the ground electronic state. M, the electronic transition moment connecting the ground and excited electronic states is a function of the nuclear coordinate (Q) and can be expanded into a Taylor series about the equilibrium position (Herzberg–Teller expansion) as follows:

$$M(Q) = M_o + \sum_j \left(\frac{\partial M}{\partial q_j}\right)_0 q_j + \ldots \quad (2)$$

Substituting the value of M in the expression for Raman transition polarizability, we get

$$\alpha_{i\to f}(E_L) = A + B + \ldots \quad (3)$$

where A and B represent Albrecht A- and B-term contributions to the Raman transition polarizability. Under the resonance condition, the A-term polarizability for the totally symmetric modes is of greater significance and higher magnitude than the B-term polarizability. Hence, in this review, we restrict ourselves only to the A-term resonance Raman scattering, which depends on the following factors:

1) The transition dipole moment, M (coordinate dependence of M is assumed to be negligible as compared to M evaluated at the equilibrium geometry),
2) The product of the vibrational overlap integrals (Franck–Condon factors), $\langle fv\rangle$ and $\langle vi\rangle$,
3) The energy denominator as given in eq. (1) that corresponds to the difference in the excitation energy and the energy gap between the ground and excited electronic states, and
4) The homogeneous broadening term, Γ, which is related to lifetime in the excited electronic state.

Thus, resonance Raman scattering has appreciable magnitude when the transition from ground to excited electronic state is electric-dipole allowed and the excitation wavelength is in resonance with a strongly-allowed absorption band. Moreover, the vibrational overlap integrals, $\langle fv\rangle$ and $\langle vi\rangle$ are non-vanishing if there is a change in the frequency upon excitation from the ground to the excited electronic state for any vibrational mode (i.e., resulting in change in shape of the potential energy surface from ground to the excited electronic state) or, if the excited state potential energy minimum is displaced relative to the ground state along any normal coordinate. Thus, large distortion along any normal coordinate, viz. changes in bond length, bond angle, etc. lead to significant resonance Raman amplitude for that coordinate, which in turn results in very high resonance Raman intensities. Hence, the displacements or distortions along the vibrational coordinate can be related to the resonance Raman intensities for that vibration.

The resonance Raman cross section, which is proportional to the product of the transition polarizability $\alpha_{i\to f}$ and its complex conjugate, can be expressed as,

$$\sigma_{i\to f}(E_L) = \frac{8\pi e^4 M^4 E_S^3 E_L}{9\hbar^4 c^4} \left| \sum_v \frac{\langle f|v\rangle\langle v|i\rangle}{E_v - E_i + E_o - E_L - i\Gamma} \right|^2, \quad (4)$$

where, e is the charge of the electron, c the velocity of light, $\hbar = h/2\pi$ (h being Planck's constant), and E_S is the energy of the scattered photon. Here E_L, E_S, E_o, E_i, E_v and Γ are in cm^{-1}, M is in Å, and $\sigma_{i\to f}$ in $Å^2$/molecule. Evaluation of the resonance Raman cross section using the sum over states approach involves summing over all the vibrational levels of the resonant electronic state. This method, therefore, requires knowledge of all the eigenstates in the excited state surface, which is therefore almost intractable for polyatomic molecules.

In the sum over states method, the absorption cross section can be expressed as

$$\sigma_A(E_L) = \frac{4\pi e^2 M^2 E_L}{3\hbar cn} \sum_v \frac{\Gamma}{\pi} \frac{|\langle v|i\rangle|^2}{(E_v - E_i + E_o - E_L)^2 + \Gamma^2}, \quad (5)$$

where n is the refractive index of the solution. The absorption cross section depends on almost similar factors as the Raman transition amplitude.

3.2. Time-dependent method

The time-dependent theory of Raman scattering[31] has an advantage over the sum over states method, in that knowledge of all the eigenstates in the excited surface is not required. Further, time-dependent approach developed by Heller[31] provides a physical picture of bulk and dynamics in the resonant excited electronic , the observe time-dependent picture, the energy den ss does not agre (4) is replaced by an exponential func on the phonon con nance Raman cross section[31] is e ed $\delta\omega$ (using LO alf- Fourier transform of the correlatio rimental va $i(t)\rangle$,

esses, ind strain. T atch bet eO2 (1 as $\frac{(E_L + E_i)t}{\hbar} - \frac{\Gamma t}{\hbar}\Big] dt \Big|^2$, the iso

$$\sigma_{i\to f}(E_L) = \frac{8\pi e^4 M^4 E_S^3 E_L}{9\hbar^6 c^4} \left| \int_0^\infty \langle f|i(t)\rangle e^{\left[\frac{(E_L + E_i)t}{\hbar} - \frac{\Gamma t}{\hbar}\right]} dt \right|^2, \quad (6)$$

where $|i(t)\rangle$ is ' evolving wavepacket on the excited electronic surface, at various intervals of time, under the influence of the excited state Hamiltonian, H_{ex}

$$|i(t)\rangle = \exp\left(-\frac{iH_{ex}t}{\hbar}\right)|i\rangle, \quad (7)$$

where $\exp(-iH_{ex}t/\hbar)$ is the time-evolution operator. The time-evolution of the wavepacket is carried out using the grid technique[32,33] as discussed in detail elsewhere[7,8].

The expression for the absorption cross section[31] in the time-dependent formalism is expressed as follows:

$$\sigma_A(E_L) = \frac{4\pi e^2 M^2 E_L}{6\hbar^2 cn} \int_{-\infty}^{\infty} \langle i | i(t) \rangle \exp\left[\frac{i(E_L + E_i)t}{\hbar} - \frac{\Gamma |t|}{\hbar}\right] dt. \quad (8)$$

In eqs (6) and (8), the dynamical information is contained in the correlation functions, $\langle f|i(t)\rangle$ and $\langle i|i(t)\rangle$. It can be illustrated schematically as shown in Figure 2. The initial wavefunction $|i\rangle$, corresponding to the zeroth vibrational level in the ground electronic state is transposed by the exciting laser (E_L) to the electronically-excited state. For simplicity, we have shown one dimensional potential energy surface representing a normal coordinate. But in reality, polyatomic molecules have various vibrational degrees of freedom, so the potential surfaces for all the Franck–Condon active modes need to be considered which would result in a complicated multi-dimensional potential energy surface. Thus, at zero time, the excitation source instantaneously promotes the molecule from the ground to the excited electronic state. The wavepacket generated in the excited electronic state (S_1) is a coherent superposition of stationary states, each multiplied by their phase factors. This transposed wavepacket is not an eigen function of the excited state Hamiltonian, and hence under its influence, it begins to move in the excited state surface. The overlap of the time-evolving wavepacket $|i(t)\rangle$ with the initial wavepacket $|i\rangle$ gives the autocorrelation function, $\langle i|i(t)\rangle$ and with the final wavefunction, $|f\rangle$ gives the Raman correlation function, $\langle f|i(t)\rangle$. At zero time, the wavepacket along all coordinates are in phase but soon they lose their phase relationship. The Fourier transform of the autocorrelation function gives the absorption spectrum and square of the half Fourier transform of the Raman correlation function gives the Raman excitation profile. The experimental factors used to compute REPs involve the integrated intensities and the vibrational frequencies corresponding to each Raman fundamental. The integrated intensities under short-time approximation is expressed as $I_R \propto \Delta^2\omega^2$, where Δ and ω are the dimensionless displacement and the frequency in wavenumbers, respectively. The dimensionless distortions in the excited state when converted to internal coordinates give an estimate of the real time dynamics in excited electronic state. Therefore, by computing the REPs and the absorption spectrum, one can learn about the structural and chemical dynamics in the excited electronic state[1,7,15].

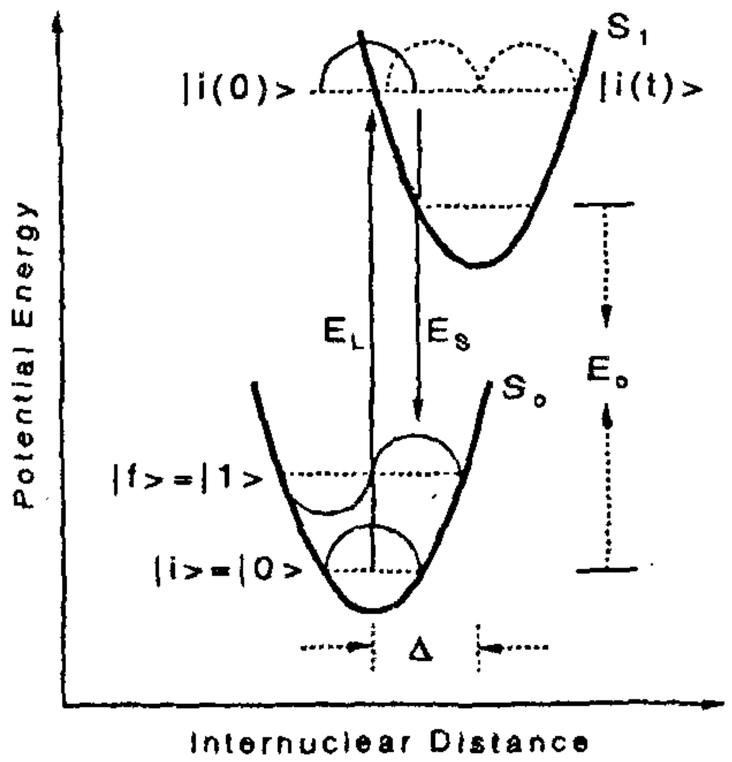

Figure 2. Schematic representation of wavepacket propagation in resonance Raman scattering.

3.3. *Effect of interference*

On photo-excitation to a particular electronic level, it is assumed in general, that the enhancement in resonance Raman intensity arises solely due to the resonant electronic state (A-term) and hence the REPs follow the electronic absorption band profile. But in practice, occasionally, there is decrease in Raman intensities as the excitation wavelength approaches the absorption maxima. Such a de-enhancement[7,8,34–47] in resonance Raman intensities may arise due to the interference from an electronic state with that of the resonant excited state. The effect of interference depends on various factors such as the energy difference between the resonant and interfering state, the transition moments of the two electronic states, nature (spin state, symmetry and polarization) of the two states involved and the vibronic coupling between them.

The effect of interference from the pre-resonant electronic state[17,48] can be approximated as follows:

$$\sigma_R(E_L, E_S) = E_L E_S^3 \{A_{pre}\}^2, \quad (9)$$

$$\{A_{pre}\}^2 = K\left[\frac{E_e^2 + E_L^2}{(E_e^2 - E_L^2)^2}\right]^2, \quad (10)$$

where E_e is the energy of the resonant electronic state and K is the coupling strength.

In this review, we consider only two extreme possibilities of resonant and pre-resonant interference. One, in which both resonant and pre-resonant terms contribute to $\alpha_\perp$, which occurs when both the excited electronic states are polarized along the same direction. Here, the depolarization ratio (ρ) is constant (~1/3) and is independent of excitation wavelength and the Raman cross section resulting from resonance and pre-resonance interference[47] is as follows:

$$\sigma_R(E_L, E_S) = \frac{8\pi E_S^3 E_L}{9\hbar^4 c^4}\left|\alpha_{res} + \alpha_{pre}\right|^2, \quad (11)$$

where α_{pre} is related to A_{pre} term by the following expression:

$$\left|\alpha_{pre}\right|^2 = \frac{9\hbar^4 c^4}{8\pi}\left\{A_{pre}\right\}^2. \quad (12)$$

The other possibility of interference occurs when the pre-resonant term contributes only to $\alpha_{\parallel}$ whereas, the resonant term contributes to $\alpha_{\perp}$, i.e. both the electronic states are polarized perpendicular to each other. In this case, the depolarization ratio (ρ) is not a constant, instead it is a function of excitation wavelength[47] and is expressed as

$$\rho = \frac{\left|\alpha_{res}\right|^2 + \frac{4}{9}\left|\alpha_{pre}\right|^2 - \frac{2}{3}(\alpha_{pre}\alpha_{res}^* + \alpha_{pre}^*\alpha_{res})}{3\left|\alpha_{res}\right|^2 + \frac{32}{9}\left|\alpha_{pre}\right|^2 + \frac{4}{3}(\alpha_{pre}\alpha_{res}^* + \alpha_{pre}^*\alpha_{res})}, \quad (13)$$

and thus, the Raman cross section can be described as

$$\sigma_R(E_L, E_S) = \frac{8\pi}{3}\left(\frac{1+2\rho}{1+\rho}\right)\times\frac{4E_S^3E_L}{15\hbar^4c^4}\left[\left|\alpha_{res}\right|^2 + \left|\alpha_{pre}\right|^2 + \frac{1}{6}(\alpha_{res}^*\alpha_{pre} + \alpha_{res}\alpha_{pre}^*)\right]. \quad (14)$$

3.4. Effect of solvent perturbation

In solution, the solute molecules are subjected to random forces arising due to their interaction with the surrounding solvent molecules, leading to significant line broadening in the absorption spectra and the resonance Raman intensities, which have been analysed on the basis of Brownian oscillator model developed by Mukamel's group[49] where the solvent coordinates are treated as displaced harmonic oscillators that are frictionally damped to different extents. Due to stochastic forces[50] exerted on the molecule in solution, it causes the energy gap between the ground and the resonant electronic state to fluctuate with time. The fluctuations of the electronic energy levels due to the influence of solvents are considered to have a Gaussian distribution and thus, can be described by the amplitude of fluctuation, D_s and the inverse time scale of the fluctuation, Λ. When the solute–solvent interaction is in the 'rapid fluctuation' limit (i.e. when the fluctuation in E_0 is very fast compared to the Raman line width), the resonance Raman cross section for the transition $|i\rangle \rightarrow |f\rangle$ is given by,

$$\sigma_{R,i\rightarrow f}(E_L) = \frac{8\pi e^4 E_S^3 E_L M^4}{9\hbar^6 c^4}\int_{-\infty}^{\infty} d\delta G(\delta) \times\left|\int_0^{\infty} dt\langle f|i(t)\rangle \exp\left[\frac{i(E_L + E_i - E_o - \delta)t}{\hbar} - \frac{\Gamma t}{\hbar} - g(t)\right]\right|^2, \quad (15)$$

where $G(\delta)$ and $g(t)$ are the inhomogeneous distribution of zero-zero energies and solvent induced broadening, respectively. In the Brownian oscillator model[49], $g(t)$ can be expressed as a sum of number of vibrations of the solvents, although the normal practice is to treat all the solvent degrees of freedom as one effective mode. When this effective mode is strongly overdamped and its frequency is very low compared to kT (k and T being Boltzmann constant and absolute temperature) which happens in the case of most strongly coupled solvent motions, $g(t)$ assumes the form

$$g(t) = \left(\frac{D_s}{\Lambda}\right)^2\left(\Lambda t - 1 + e^{-\Lambda t}\right) + i\left[\frac{(\lambda_s/\hbar)}{\Lambda}\right]\left(1 - e^{-\Lambda t}\right), \quad (16)$$

where

$$D_s = \left[\left(\frac{\lambda_s}{\hbar}\right)\omega_s(2\bar{n}+1)\right]^{1/2}, \quad (17)$$

$$\Lambda = \frac{\omega_s^2}{f}, \quad (18)$$

$$\lambda_s = \frac{\omega_s\Delta_s^2}{2}. \quad (19)$$

ω_s and Δ_s being the frequency of the vibration and the geometry change between the ground and excited state potential minima in dimensionless normal coordinates for the solvent, respectively, f is the friction coefficient in units of frequency and $\bar{n}$ is the thermal average occupation number of the solvent. Normally, the shift and broadening of the charge transfer absorption band is described by the total reorganization energy, λ and broadening parameter D which have contributions from both the high frequency molecular modes and low frequency solvent modes. Thus,

$$\lambda = \lambda_v + \lambda_s, \quad (20)$$

where λ_v is the intra-molecular vibrational reorganization energy and is expressed as follows:

$$\lambda_v = \frac{\omega\Delta^2}{2} \tag{21}$$

ω and Δ being the frequency of the vibration and the geometry change between ground and excited state potential minima in dimensionless normal coordinates of the solute molecule, respectively. Similarly, the total broadening parameter,

$$D^2 = D_v^2 + D_s^2, \tag{22}$$

$$D_v = \left[\left(\frac{\lambda_v}{\hbar}\right)\omega(2\bar{n}_v + 1)\right]^{1/2}, \tag{23}$$

$\bar{n}_v$ being the thermal average occupation number of the molecule. The solvent reorganization energy (λ_s) and the internal reorganization energies (λ_v) play an important role in determining the rates of electron transfer reactions.

Similarly, the absorption cross section for a molecule in solution is given as

$$\sigma_A(E_L) = \frac{4\pi e^2 E_L M^2}{3\hbar^2 cn}\int_{-\infty}^{\infty} d\delta G(\delta) \times \int_{-\infty}^{\infty} dt\langle i|i(t)\rangle \exp\left[\frac{i(E_L + E_i - E_o - \delta)t}{\hbar} - \frac{\Gamma t}{\hbar} - g(t)\right]. \tag{24}$$

For the time-dependent calculations, the assumptions are that there is no change in normal coordinate on electronic excitation (no Duschinsky rotation). Moreover, the excited state potential surfaces are assumed to be harmonic, with no change in frequencies and differ from the ground state surface by only a constant term in energy (zero–zero energy, E_0) and is displaced by an amount Δ (in dimensionless units) with respect to the ground state minimum.

The displacement parameters used to fit the REPs and the absorption spectrum are usually expressed in terms of dimensionless normal coordinates. But actual atomic motions in internal coordinates are required in order to understand the structural distortions and dynamics in the excited electronic state. Thus, dimensionless normal coordinates can be converted to internal coordinates using the normal-mode vectors as discussed previously[7].

4. Applications of RR spectroscopy

RR intensities have been commonly used to study various photochemical processes, viz. photodissociation, pericyclic ring opening reactions, sigmatropic shifts, isomerization as well as electron transfer reactions. In this review, we give a brief account of various photochemical reactions studied using RR spectroscopy in combination with Heller's time-dependent wavepacket dynamical approach[31].

4.1. Photodissociation dynamics

The time-dependent picture of RR scattering has been successfully utilized over the recent years to gain information regarding the short-time dynamics of photodissociating molecules both in the gas phase as well as in solutions. Methyl iodide[51], iodine[52], nitromethane[53], *n*-propyl iodide[54], ethyl iodide, isopropyl iodide, tertiary-butyl iodide[47,55], diiodomethane[56,57], chloroiodomethane[56], bromoiodomethane[56], triiodide anion[58] and 1,1,1-trifluoro-2-iodoethane[59] are some of the molecules undergoing photodissociation, that have been studied using RR spectroscopy. In a recent article, Kwok *et al.*[59] have studied femtosecond photodissociation dynamics of 1,1,1-trifluoro-2-iodoethane in the FC region. They have recorded the RR spectra of 1,1,1-trifluoro-2-iodoethane in cyclohexane solution, with excitation wavelength resonant to the A-band absorption (273.9, 282.4 and 299.1 nms). They have shown that during the early stages (i.e. within 15 fs) of photodissociation in the FC region, as the C–I bond breaks, the CF_3CH_2 radical moves toward a more planar geometry about the CH_2 carbon atom. Moreover, the C–C bond becomes longer, CCI angle becomes smaller, the HCH and CCH angles become larger and two of FCC angles (out of CCI plane) become larger while third FCC angle (in the CCI plane) becomes smaller with some motion in the FCF angles and C–F bond length.

4.2. Structural dynamics

Isomerization and pericyclic rearrangement reactions, including ring opening reactions, sigmatropic shifts, etc. have been studied using this technique.

Isomerization dynamics. The excited state isomerization dynamics and the structural distortions associated with it, in case of *cis*-stilbene have been studied using both RR[60] and TR[3] spectroscopy[61]. In this review, the discussion is restricted to our results on photo-induced isomerization of *trans*-azobenzene[7,9]. In azobenzene, due to the presence of a lone pair of electrons on the N atom, there are two possible routes of isomerization[62] as shown in Figure 3, one by rotation about the central N=N double bond and the other by inversion about one of the N-sites via sp-hybridized transition state.

Trans-azobenzene in CCl_4 consists of a lowest energy symmetry forbidden ($2^1A_g \leftarrow 1^1A_g$) transition, in

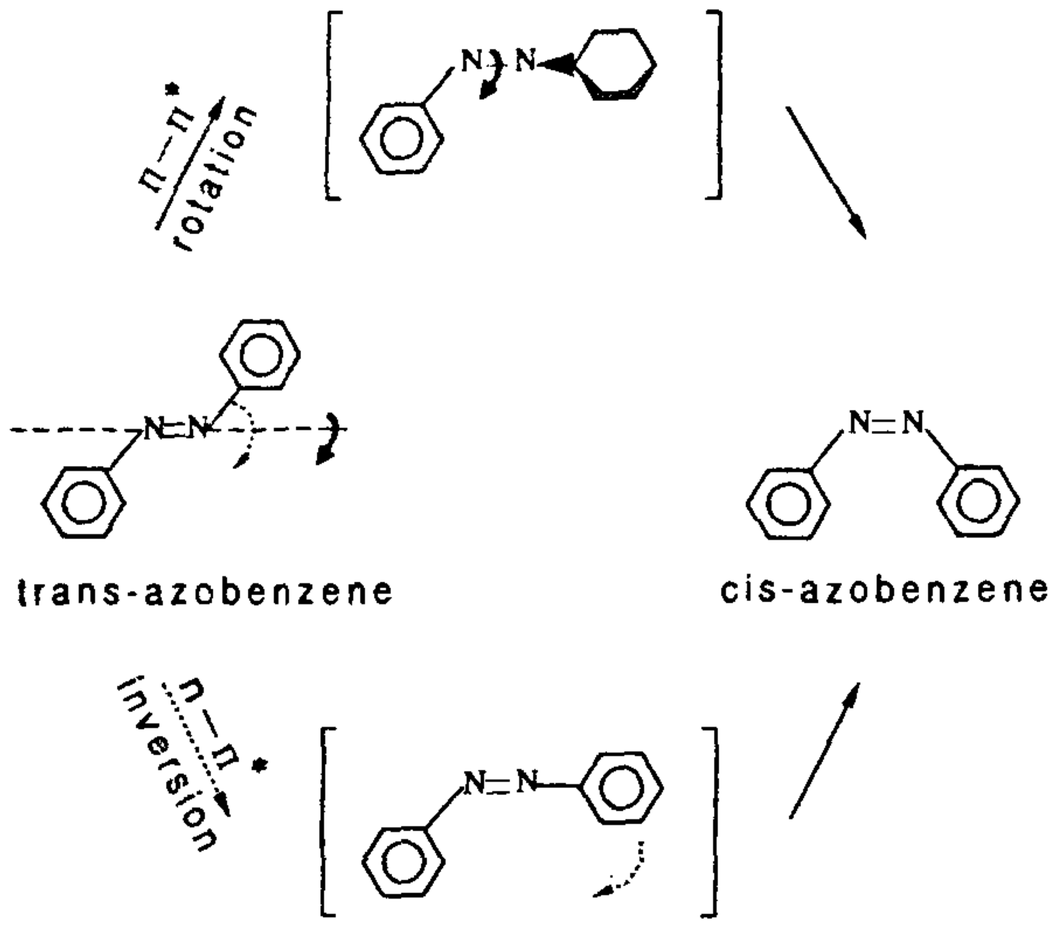

Figure 3. Proposed pathways for isomerization of *trans*-azobenzene to *cis*-azobenzene.

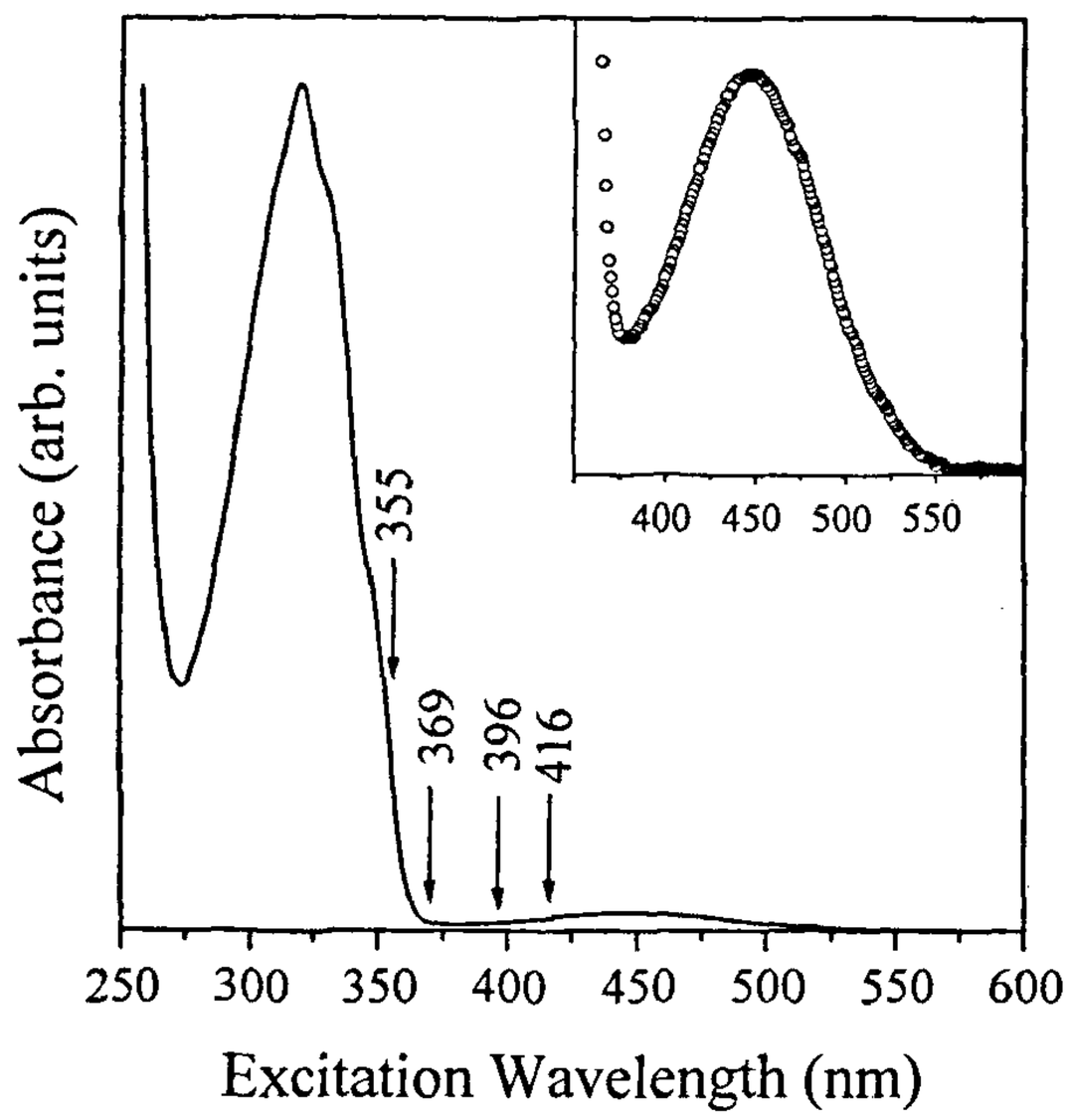

Figure 4. Absorption spectrum of *trans*-azobenzene in carbon tetrachloride solution. The weak band from 400–600 nm corresponds to $(2^1A_g \leftarrow 1^1A_g)$ electronic transition and the strong band in the region 250–400 nm is due to $(1^1A_u \leftarrow 1^1A_g)$ transition. Inset shows the expanded form of $(2^1A_g \leftarrow 1^1A_g)$ transition. The arrows indicate the excitation wavelengths (in nm) used to carry out the pre-resonance Raman measurements.

addition to the strongly allowed $(1^1A_u \leftarrow 1^1A_g)$ transition as shown in Figure 4. A comprehensive study on the isomerization quantum yields of sterically hindered

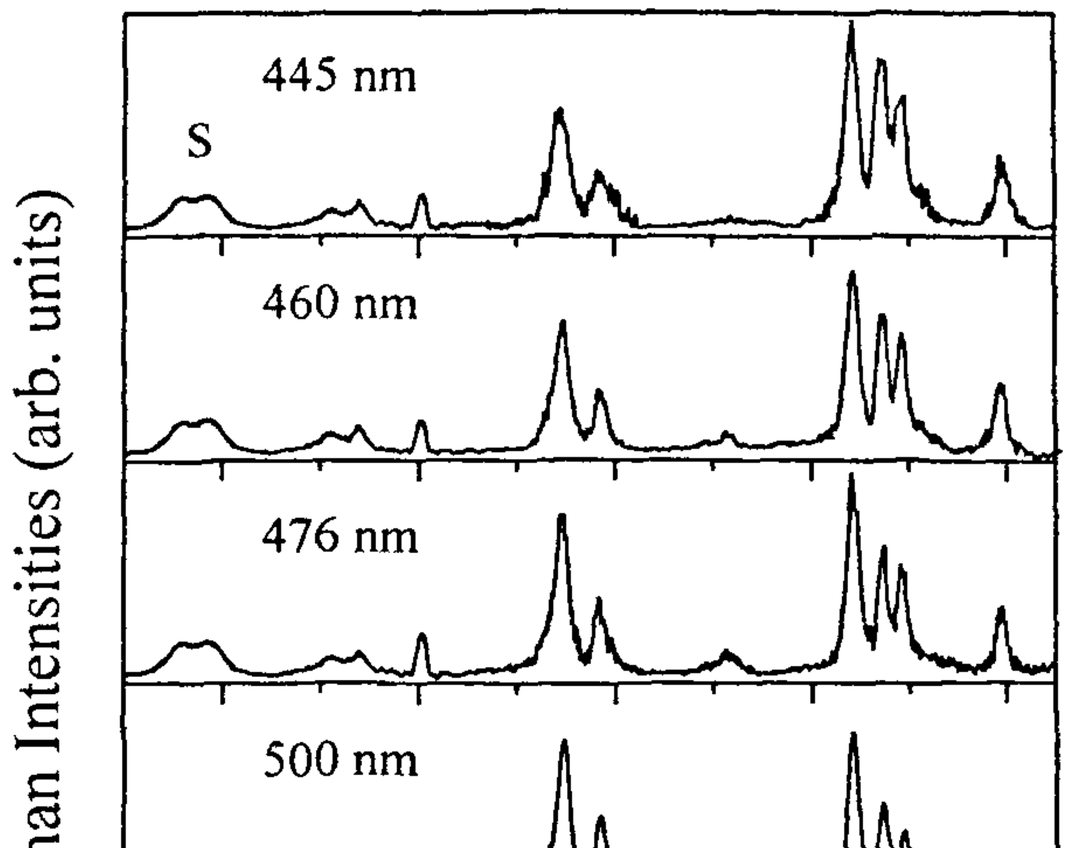

Figure 5. Resonance Raman spectra of *trans*-azobenzene in carbon tetrachloride solution with excitation wavelengths, 445, 460, 476, 500, 532 and 597 nm.

azobenzenes by Rau *et al.*[63,64] has indicated that the mechanism of isomerization critically depends on the excitation wavelength. *Trans*-azobenzene undergoes photoisomerization via inversion mechanism when excited to the lowest energy $(2^1A_g \leftarrow 1^1A_g)$ transition and by rotational mechanism upon excitation to the higher energy $(1^1A_u \leftarrow 1^1A_g)$ transition. The inset in Figure 4 shows the expanded form of $(2^1A_g \leftarrow 1^1A_g)$ transition. Though $(2^1A_g \leftarrow 1^1A_g)$ transition is symmetry forbidden, the Raman intensities observed in solution are ascribed to pure resonance[7,9,27]. The absence of vibrational structure in the low temperature absorption spectrum[65,66] corresponding to $(2^1A_g \leftarrow 1^1A_g)$ transition of *trans*-azobenzene implies that isomerization occurs much more rapidly than vibrational recurrences to the FC region.

The Raman spectra of *trans*-azobenzene in CCl_4 resonant with $2^1A_g \leftarrow 1^1A_g$ electronic transition using few excitation wavelengths, viz. 445, 460, 476, 500, 532 and 597 nm are shown in Figure 5. The spectra at all wavelengths have been normalized with respect to the

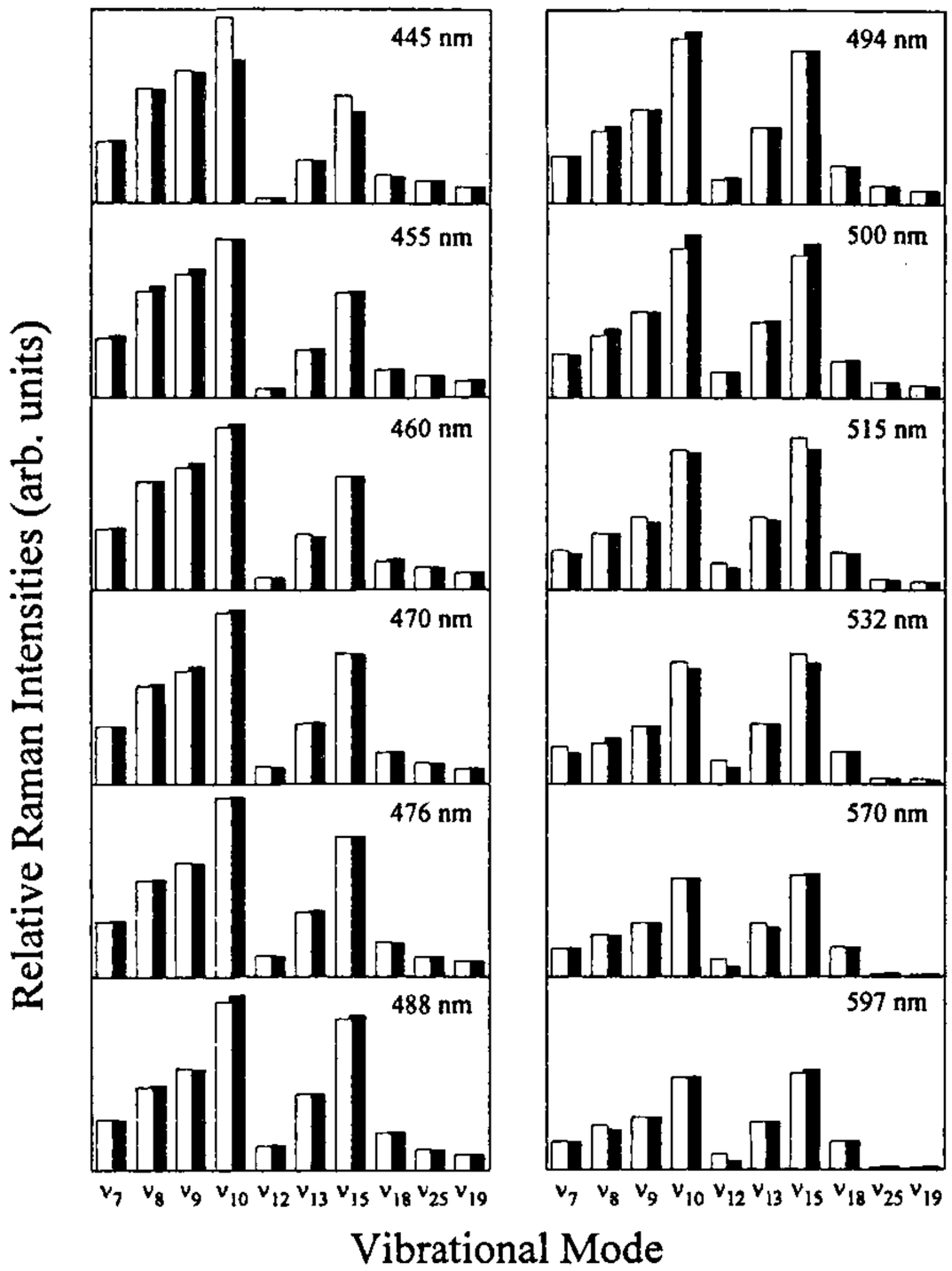

Figure 6. Comparison of the experimental (open bars) and calculated (solid bars) of the relative Raman intensities at excitation wavelengths, viz. 445, 455, 460, 470, 476, 488, 494, 500, 515, 532, 570 and 597 nm in the ($2^1A_g \leftarrow 1^1A_g$) absorption region of *trans*-azobenzene in carbon tetrachloride solution.

CCl_4 doublet (marked *S* in the figure) appearing at 762 and 791 cm^{-1}, respectively. The fundamentals observed in the region 800–1600 cm^{-1} are, 912 (ν_{19}), 939 (ν_{25}), 1000 (ν_{18}), 1142 (ν_{15}), 1181 (ν_{13}), 1312 (ν_{12}), 1439 (ν_{10}), 1470 (ν_9), 1491 (ν_8) and 1592 (ν_7) cm^{-1}. Most intense Raman bands correspond to the N=N and C–N stretch appearing at 1439 and 1142 cm^{-1}, followed by 1491, 1470, 1592 and 1181 and 1000 cm^{-1}. Three weak bands are observed at 912, 939 and 1312 cm^{-1}. In Figure 6, the relative Raman intensities (open bars) of these normal vibrations at each excitation wavelength have been shown. It is observed from the figure that as the excitation wavelength is tuned to resonance with the lowest energy transition, with λ_{max} at 445 nm, the intensities of the fundamental modes increase but as it approaches the absorption maxima, de-enhancement is observed for few of the vibrations, viz. 1000, 1142, 1181, 1312 and 1439 cm^{-1}. This led us to believe that Raman intensities of these modes may arise not only from the resonant electronic state but have contributions from the higher lying electronic state.

Table 1. Raman frequencies (ω in cm^{-1}), dimensionless displacements (Δ) in the resonant electronic state and the vibrational assignments of *trans*-azobenzene

Vibrational mode	Frequency (ω in cm^{-1})	Dimensionless displacement (Δ)	Vibrational assignments
ν_7	1592	0.43	ν(C–C)
ν_8	1491	0.59	ν(C–C)
ν_9	1470	0.68	ν(C–C)
ν_{10}	1439	0.86	ν(N=N)
ν_{12}	1312	0.25	δ(C–H)
ν_{13}	1181	0.60	ν(C–C)
ν_{15}	1142	0.93	ν(C–N)
ν_{18}	1000	0.54	δ(C–C)
ν_{25}	939	0.42	γ(C–H)
ν_{19}	912	0.39	δ(C–C)

ν, stretch; δ, in-plane bend; γ, out-of-plane bend.
Zero–zero energy, $E_{00} = 20645\ cm^{-1}$; electronic transition dipole, $M = 0.8$ Å; life time broadening, $\Gamma = 200\ cm^{-1}$ and solvent induced broadening, $\theta = 700\ cm^{-1}$.

Based on our simulated displacements as shown in Table 1, the isomerization dynamics can be inferred. Under $2^1A_g \leftarrow 1^1A_g$ electronic transition as shown in the table, the vibrational modes, viz. 1439 and 1142 cm^{-1} have maximum displacements in the excited state and these modes correspond to ν(N=N) and ν(C–N) stretch, respectively and a smaller displacement is observed for the ring stretch mode at 1491 cm^{-1} which is in contrast to the case of *cis*-stilbene[60] where rotation is the only way of isomerization. This suggests that inversion (and not rotation) is the most likely route of isomerization in case of *trans*-azobenzene under $2^1A_g \leftarrow 1^1A_g$ excitation. The parameters, viz. zero–zero energy ($E_0 = 20645\ cm^{-1}$), electronic transition dipole ($M = 0.8$ Å), life time broadening ($\Gamma = 200\ cm^{-1}$) and solvent induced broadening ($\theta = 700\ cm^{-1}$), used to fit the REPs are also included in the table.

In order to study the isomerization dynamics, a detailed normal coordinate analysis of *trans*-azobenzene has been carried out using density functional theory (BP86) with 6-31G* basis set[67]. From the knowledge of the ground state normal modes of *trans*-azobenzene at their equilibrium geometry as well as the dimensionless displacements, the change in internal coordinates as a function of time (t) has been calculated. Only changes in early times (within 30 fs) are considered because the multimode correlation function decays in 30 fs. In Figure 7, we have shown a schematic representation of the isomerization dynamics of *trans*-azobenzene at time (t), (a) 0 fs, (b) 20 fs and (c) 30 fs, respectively. The magnitude of the displacement values has been multiplied 20 times their true cartesian displacements for better visualization. From the figure it is evident that with time, during the inversion process about one of the N atoms, C–N elongates and N=N undergoes reduction in length. We also find that the C–C bond adjacent to the C–N bond reduces in length, C–C–N angle becomes smaller

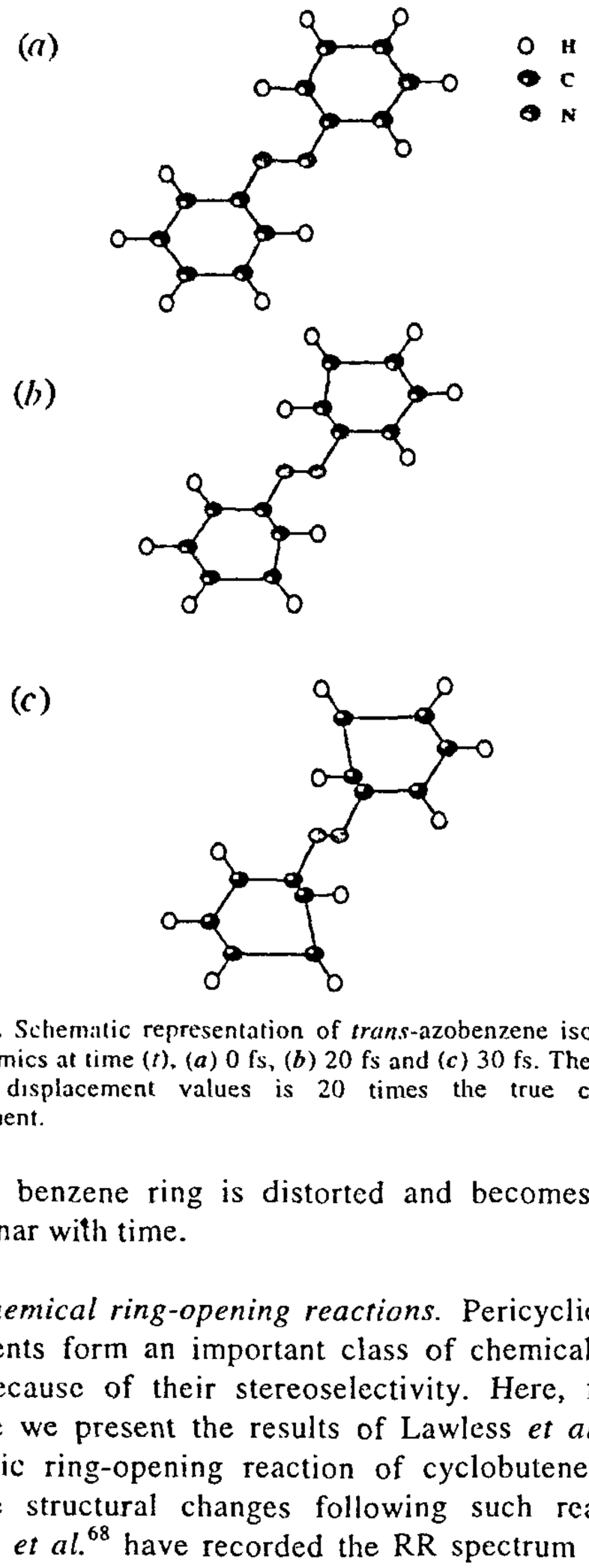

Figure 7. Schematic representation of *trans*-azobenzene isomerization dynamics at time (t), (a) 0 fs, (b) 20 fs and (c) 30 fs. The magnitude of displacement values is 20 times the true cartesian displacement.

and the benzene ring is distorted and becomes more non-planar with time.

Photochemical ring-opening reactions. Pericyclic rearrangements form an important class of chemical reactions because of their stereoselectivity. Here, for an example we present the results of Lawless *et al.*[68] on pericyclic ring-opening reaction of cyclobutene (CB) and the structural changes following such reaction. Lawless *et al.*[68] have recorded the RR spectrum of CB excited at 200 nm. CB shows intense band at 1563 cm^{-1} corresponding to C=C stretch indicative of increase in bond length along this coordinate upon photo-excitation. A strong band is also observed at 1110 cm^{-1}, corresponding to aliphatic CH_2–CH_2 stretch, which is consistent with the fact that this bond breaks during the course of photochemical reaction. The fundamental of the non-totally symmetric CH_2 twist mode is not observed but significant intensity is observed for its overtone. This indicates that following excitation, evolution occurs in the FC region along the Woodward–Hoffmann predicted disrotatory ring-opening reaction coordinate.

Sigmatropic shift in 1,3,5-cyclohepta-triene (CHT). Sigmatropic shifts represent a class of pericyclic reactions where structural changes occur by migration of σ bonds. The photochemical H migration of 1,3,5-cycloheptatriene (CHT) has been studied by Reid *et al.*[68]. They have shown the RR spectrum of CHT obtained at 257 nm excitation. The RR spectrum shows that majority of the scattering intensity is observed for the in- and out-of-plane ethylenic modes at 1536 and 1610 cm^{-1} as well as ring-planarization modes at 225, 354 and 419 cm^{-1}. No intensity is observed for the symmetric methylene CH stretch. Thus, in CHT, excited state evolution suggests that a planar or near-planar geometry is established before the H-migration occurs.

4.3 Resonance Raman de-enhancement

De-enhancement or antiresonance in the resonance Raman intensities[7,8,34-47,69] usually arises due to interference from closely-lying electronic states, have been observed for a number of systems, viz. HI, transition metal complexes [$Co(en)_3^{3+}$, $PdBr_4^{2-}$, etc.], ethyl, isopropyl, tertiary-butyl iodides, *trans*-azobenzene, etc. In this review, we discuss briefly resonance de-enhancement observed in case of *trans*-azobenzene. In *trans*-azobenzene, de-enhancement of Raman intensity is observed near the maxima of the resonant $2^1A_g \leftarrow 1^1A_g$ electronic transition. This arises due to interference from the closely lying $1^1A_u \leftarrow 1^1A_g$ electronic transition. In order to account for the effect of interference from the pre-resonant electronic state which corresponds to $1^1A_u \leftarrow 1^1A_g$ electronic transition with maxima near 320 nm, the depolarization ratios (ρ) were measured as a function of excitation wavelength. The values of ρ for the N=N stretching mode is found to be 0.31 (at 445 nm), 0.34 (at 476 nm), 0.36 (at 532 nm) and 0.33 (at 570 nm). These values of ρ remain almost constant (i.e. nearly equal to 1/3) with differing excitation wavelengths, implying that the pre-resonant state may be contributing to the same component of the transition polarizability tensor ($\alpha_\perp$) as does the resonant state. Thus, it is assumed that both the pre-resonant and the resonant electronic states are polarized perpendicular to the N=N axis, which is supported by the magnetic circular dichroism result[70]. The sign of the transition polarizability tensor depends on the direction of the actual geometry change occurring along a particular normal coordinate. Here, in the resonant state there is a reduction in N=N bond length since the molecule undergoes inversion about the N atom. Whereas, in the pre-resonant state, *trans*-azobenzene is known to isomerize via rotation[63], and thus, it is assumed that the N=N bond length increases. Therefore, the polarizability tensor elements ($\alpha_\perp$) are considered to be opposite in sign in the two excited electronic states. The pre-resonance Raman spectra of *trans*-azobenzene using excitation wavelengths, 355, 369, 396 and 416 nm are plotted in Figure 8. The observed fundamentals appear at 1000,

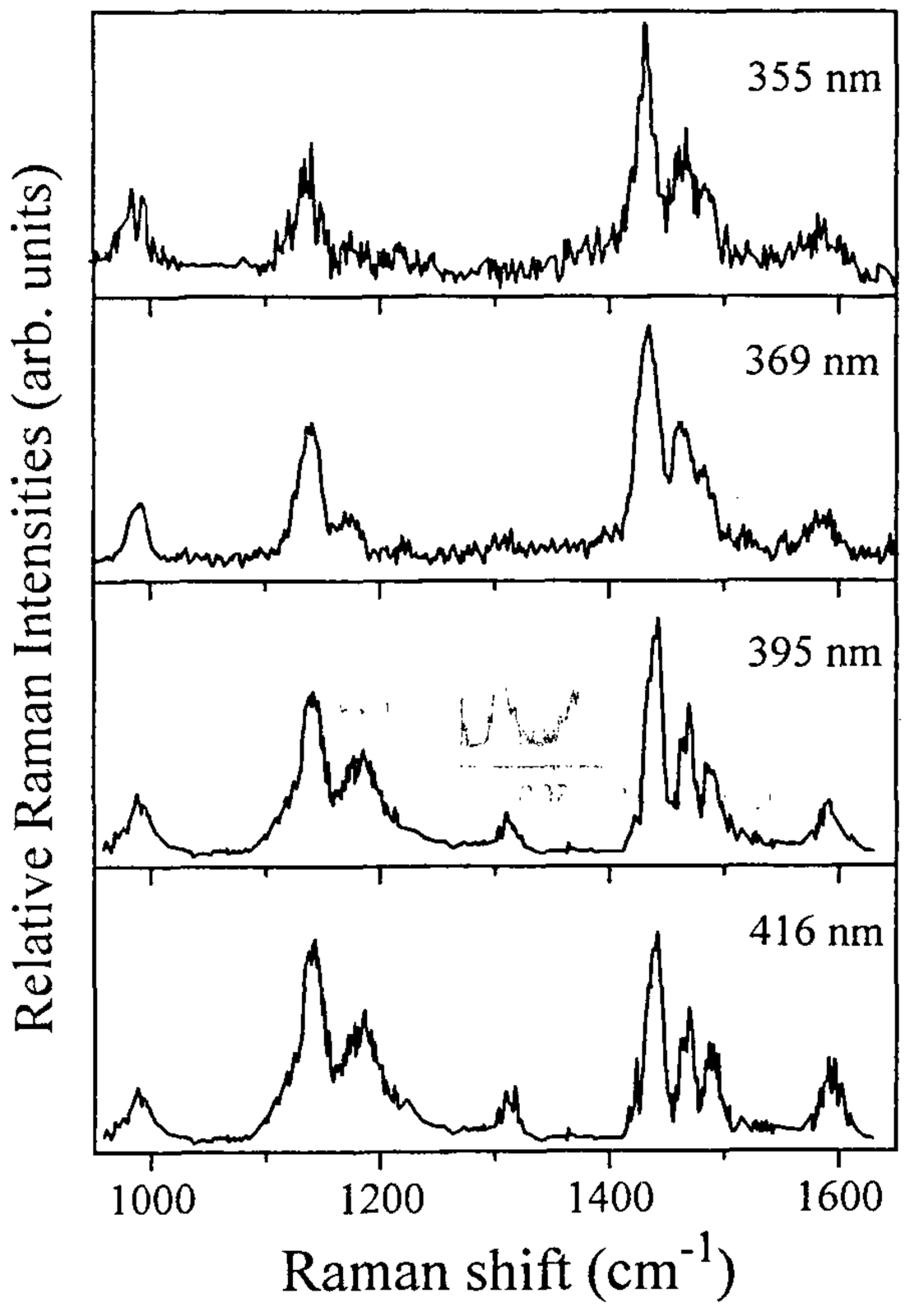

Figure 8. Pre-resonance Raman spectra of trans-azobenzene in carbon tetrachloride solution with excitation wavelengths, 355, 369, 395 and 416 nm.

1142, 1181, 1312, 1439, 1470, 1491 and 1591 cm^{-1}. Of these modes, as shown in Figure 6, 1439, 1312, 1181, 1142 and 1000 cm^{-1} show resonance de-enhancement. These are fit to a single A-term frequency dependence[17] using eqs (9) and (10) by varying the coupling strength (K) and the energy for the pre-resonant state (E_e). A good fit is obtained at $E_e = 34100\ cm^{-1}$, indicating that the pre-resonant component indeed contributes to the same Raman polarizability term ($\alpha_\perp$) as the resonant term. The transition polarizability component due to the pre-resonant electronic state (α_{pre}), has significant magnitude when extrapolated to the region of the resonant electronic state. As a result of this, it interferes destructively with the Raman polarizability component, α_{res} from the resonant electronic transition, leading to de-enhancement in the REPs of various vibrational modes of *trans*-azobenzene.

The excitation profiles for the ten Raman active modes were simulated. In all these simulations, the contribution from the pre-resonant state has been taken into account. In Figure 6, we have shown the simulated relative Raman intensities (solid bars) for all the ten normal vibrations of *trans*-azobenzene along with the experimentally-observed intensities, at all the excitation wavelengths. A good agreement between the calculated and experimental intensities for all the vibrational modes at different excitation wavelengths confirm that the assumptions considered for the simulations are reasonable.

4.4. Electron transfer reactions

Systems undergoing photo-induced electron transfer reactions have also been studied using RR spectroscopy in order to extract valuable information regarding reorganization energies which play a major role in electron transfer reactions. Excitation to the charge transfer (CT) state leads to a rapid change in charge distribution of the solute. Thus, the surrounding solvent molecules have to reorient themselves to adjust to the changes in the solute charge distribution. The role the solvent plays in controlling the electron transfer reaction critically depends on how fast or slow the solvent responds to the changes in solute charge distribution[71–75]. The changes in the properties of the solvent (viz. polarity, polarizability, etc.) is thus expected to have a dramatic influence on the excited state structure and dynamics of the solute and this can be easily monitored using RR spectroscopy[49,76–85].

Intra and inter-molecular electron transfer reactions are commonly observed in various biological, inorganic and organic chemical systems. Application of RR spectroscopy to these electron transfer reactions has been an active area of research in the recent years. In particular, importance of RR spectroscopy in understanding ultrafast electron transfer process has been described by Myers[83] and Barbara *et al.*[85]. A few examples of Raman studies on electron transfer reactions observed in the literature include hexamethylbenzene/tetracyanoethylene[78,80], biferrocene[86], $[Pt_2(\mu\text{-dppm})_2(\mu\text{-PhC}{\equiv}C)(PhC{\equiv}C)_2]^+$ (ref. 84), $[Pt(dppm)_2(PhC{\equiv}C)_2]$ (ref. 84), $(NH_3)_4Ru(2,2'\text{-bpy})^{2+}$ (ref. 87), 4-cyano-N-methylpyridinium[88], etc. In this review, we discuss in brief the influence of solvent on the photo-induced intramolecular electron transfer reaction of a donor–acceptor molecule, viz. 4-dimethylamino,4'-nitro-azobenzene (DA), the structure of which is shown in Figure 9. DA is very solvent sensitive, leading to a bathochromic shift of the absorption maxima from 453 nm in a non-polar solvent (CCl_4) to 493 nm in a polar solvent (benzonitrile) as shown in Figure 10. The arrows marked in the figure indicate the excitation wavelengths used for the resonance Raman experiments. This large shift in the absorption maxima with the increase in solvent polarity is attributed to the net stabilization of the charge separated FC excited state (S_1) relative to the ground state. The

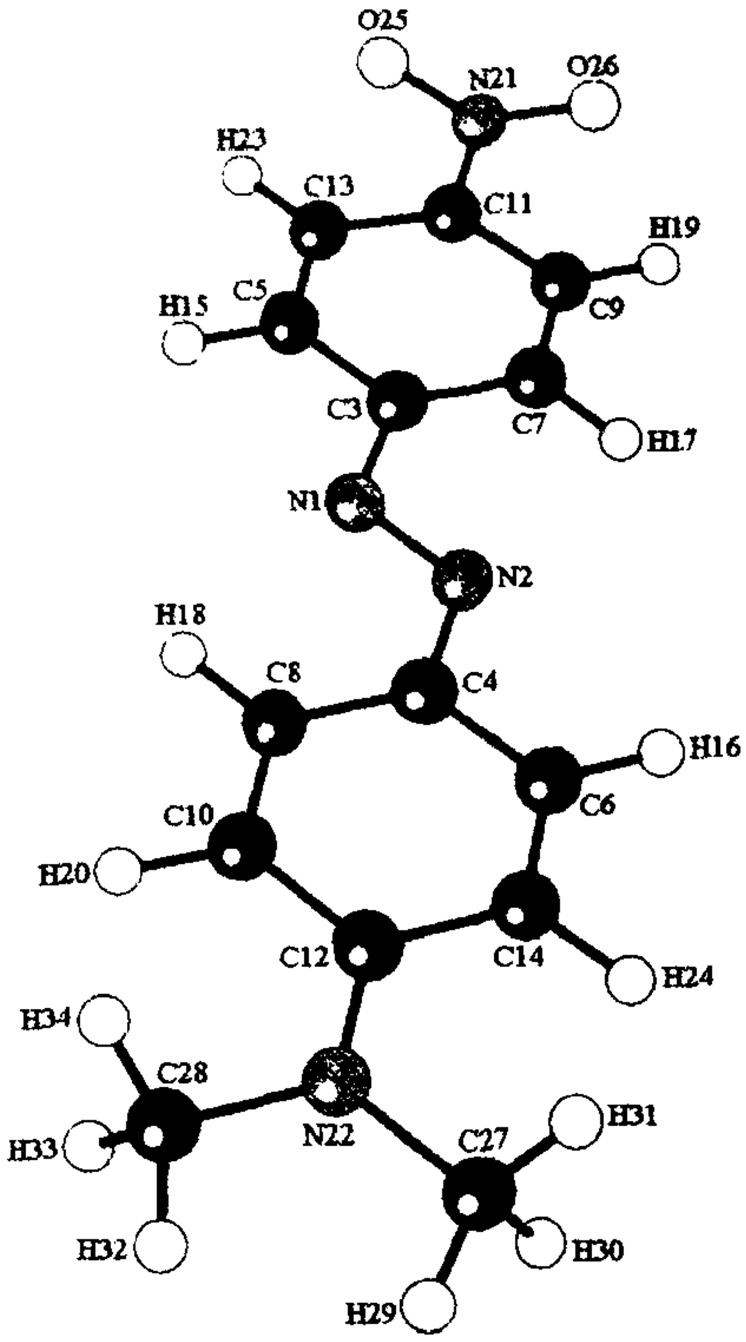

Figure 9. Geometry and atom numbering of 4-dimethylamino, 4′-nitro-azobenzene (DA).

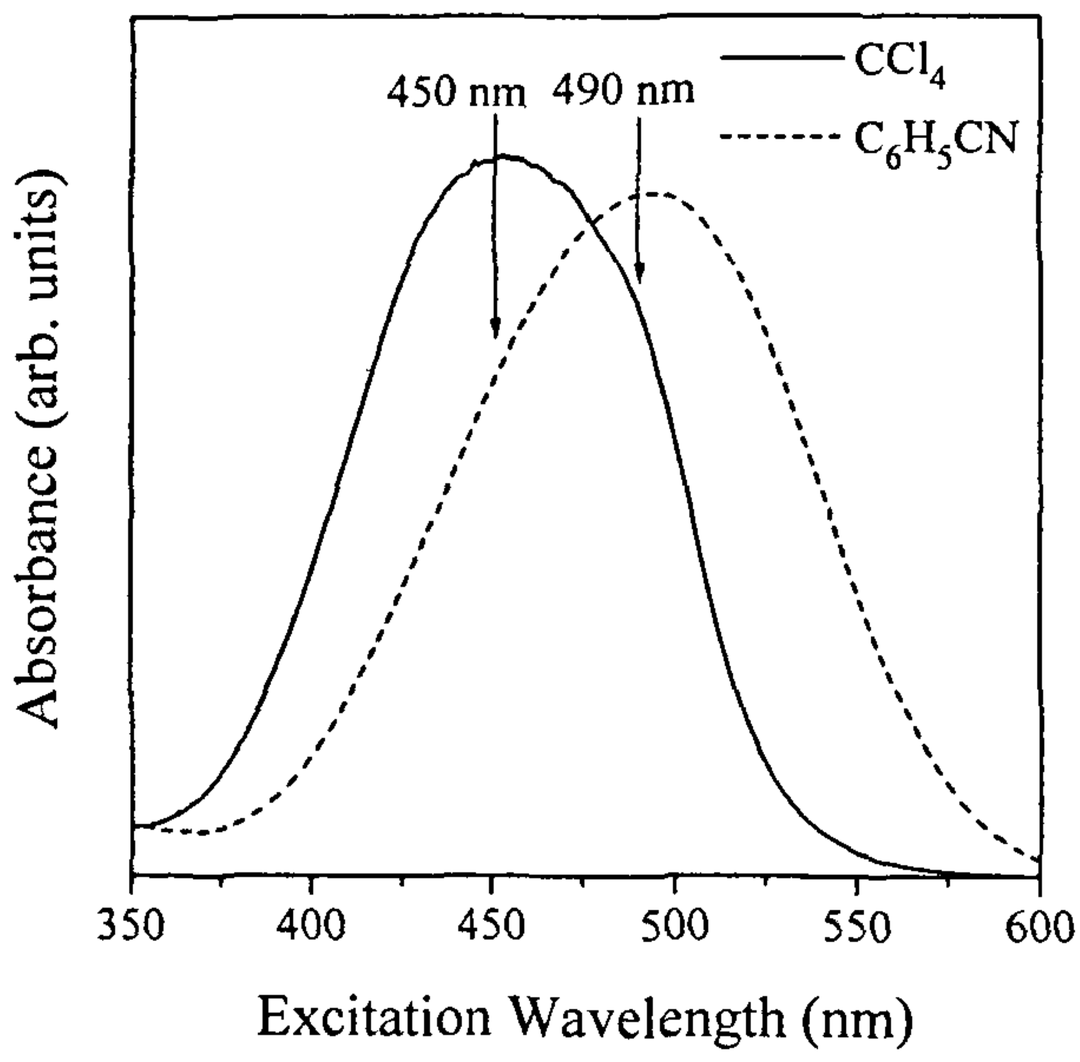

Figure 10. Absorption spectrum of 4-dimethylamino, 4′-nitro-azobenzene (DA) in carbon tetrachloride (solid line) and benzonitrile (dashed line). The arrows indicate the excitation wavelengths (in nm) used to carry out the resonance Raman measurements.

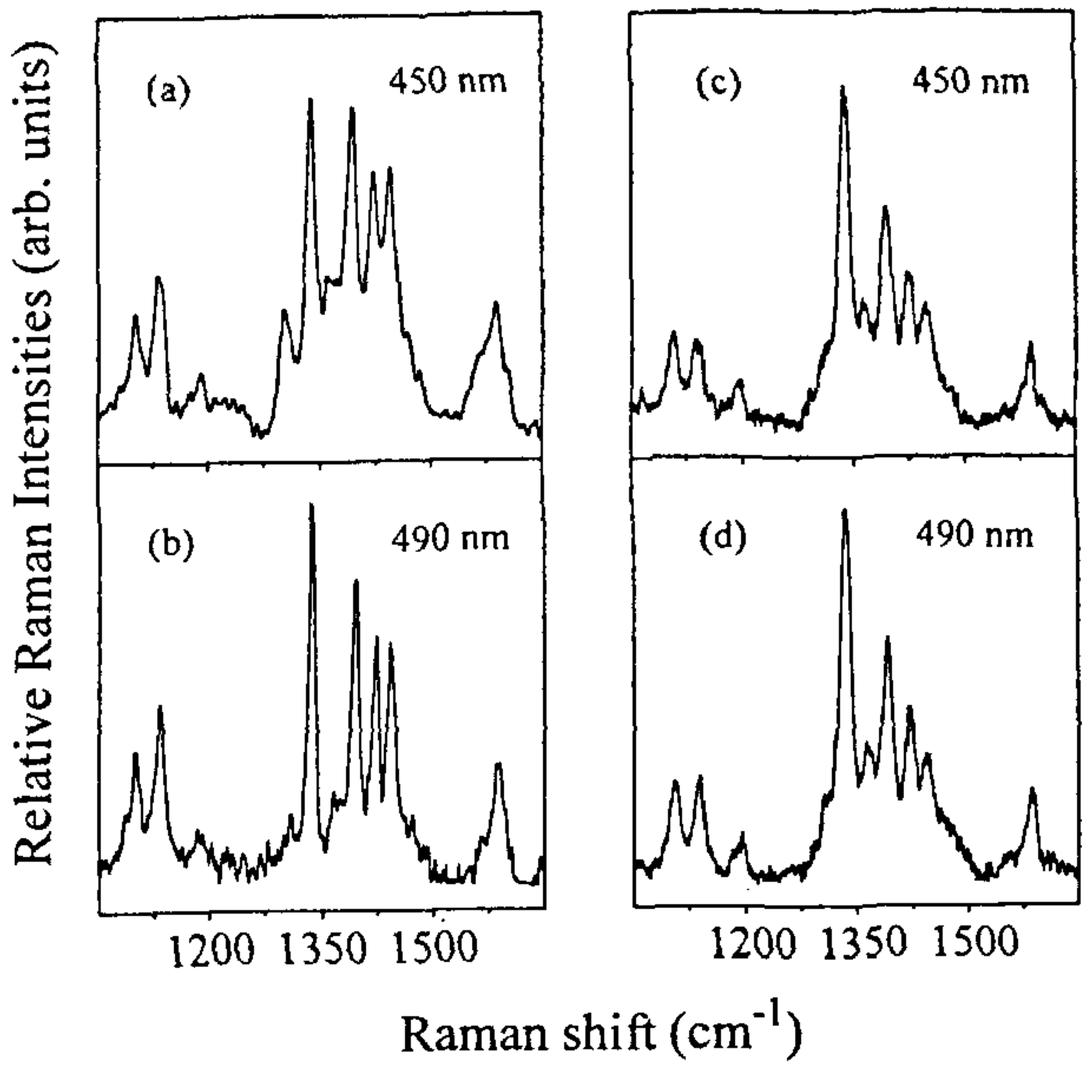

Figure 11. Resonance Raman spectra of 4-dimethylamino,4′-nitro-azobenzene (DA) in carbon tetrachloride (*a* and *b*) and benzonitrile (*c* and *d*) with excitation wavelengths, 450 and 490 nm.

magnitude of the shift of the absorption maxima depends on the extent of the change in solute dipole moment during the transition from the ground state to the excited state, the value of solvent dipole moment, the extent of solute–solvent interaction as well as the electronic polarization of the surrounding solvent molecules caused by the dipolar solute molecules. Since the room temperature absorption spectra of DA in solutions of CCl_4 and benzonitrile are diffused and not vibrationally resolved, very little information can be obtained regarding vibrational structural aspects. Hence, in order to get vibrational mode-specific information of DA, we have recorded its Raman spectra, in resonance with the charge transfer (CT) transition in the solvents specified above.

Resonance Raman spectra of DA in CCl_4 and C_6H_5CN were recorded with excitation wavelengths 450 and 490 nm by scanning a tunable laser pulse from an OPO and are shown Figure 11 *a–d*. The spectra of DA in CCl_4 (Figure 11 *a* and *b*) were normalized with respect to the CCl_4 doublet appearing at 762 and 791 cm^{-1}. Similarly, the RR spectra of DA in C_6H_5CN [Figure 11 *c* and *d*] were normalized relative to the solvent band at 1000 cm^{-1}. The fundamentals observed in the region 1000–1600 cm^{-1} for DA in CCl_4 (benzonitrile) are 1110 (1106), 1137 (1140), 1197 (1195), 1340 (1336), 1399 (1393), 1427 (1422), 1445 (1447) and 1595 (1587) cm^{-1}. The figure shows enormous increase in intensity mainly for the bands observed at 1340 (1336), 1399 (1393), 1427 (1422) and 1445 (1447) cm^{-1} on go-

ing from 450 to 490 nm in both the solvents mentioned above. The most intense Raman bands appearing at 1340 (1336) and 1399 (1393) cm^{-1} correspond to NO_2 stretch and N=N stretch, indicating the fact that these modes are strongly coupled to the charge transfer (CT) transition. We propose to apply RR intensity analysis using Heller's wave packet approach with the inclusion of solvent effect as discussed in §3 to the azo dye undergoing photo-induced CT transition in order to understand the displacements and the reorganization energy contribution of each vibrational mode associated with the transition. This also requires the knowledge of normal modes of DA, which has been carried out using density functional method. Raman scattering intensity provides information on the distortions of the FC active modes in the excited electronic state and hence on the strength of coupling of the intra-molecular vibrations and the solvent coordinate to the electron transfer process, referred to as internal and solvent reorganization energy. An analysis of the REPs give an estimate of the parameters, viz. vibrational and solvent reorganization energies which are very important in understanding solvent control of electron transfer reactions.

1. Myers, A. B., in *Laser Techniques in Chemistry* (eds Myers, A. B. and. Rizzo, T. R.), John Wiley and Sons, New York, 1995, vol. 23, p. 325.
2. Hamaguchi, H., in *Vibrational Spectra and Structure* (ed. Durig, J. R.), Elsevier, Amsterdam, 1987, vol. 16, p. 228.
3. Hamaguchi, H., in *Advances in Infrared and Raman Spectroscopy* (eds Clark, R. J. H. and Hester, R. E.), John Wiley and Sons, New York, 1985, vol. 12, p. 273.
4. Tripathi, G. N. R., in *Time Resolved Spectroscopy* (eds Clark, R. J. H. and Hester, R. E.), John Wiley and Sons, New York, 1989, vol. 18.
5. Atkinson, G. H., in *Advances in Infrared and Raman Spectroscopy* (eds Clark, R. J. H. and Hester, R. E.), John Wiley and Sons, New York, 1982, vol. 9, p. 1.
6. Biswas, N., Umapathy, S., Kalyanaraman, C. and Sathyamurthy, N., *Proc. Indian Acad. Sci.*, 1995, **107**, 233.
7. Biswas, N. and Umapathy, S., *J. Chem. Phys.*, 1997, **107**, 7849.
8. Biswas, N. and Umapathy, S., *Pramana – J. Phys.*, 1997, **48**, 937.
9. Biswas, N. and Umapathy, S., *Chem. Phys. Lett.*, 1995, **234**, 24.
10. Anandhi, R., Balakrishnan, G., Mohandas, P. and Umapathy, S., *Laser Chemistry*, 1997, in press.
11. Balakrishnan, G. and Umapathy, S., *J. Chem. Soc. Faraday Trans*, 1997, **93**, 4125.
12. Balakrishnan, G. and Umapathy, S., *Chem. Phys. Lett.*, 1997, **270**, 557.
13. Balakrishnan, Mohandas, P. G. and Umapathy, S., *J. Phys. Chem.*, 1996, **100**, 16472.
14. Anandhi, R., Balakrishnan, G. and Umapathy, S., *Curr. Sci.*, 1993, **65**, 332.
15. Myers, A. B. and Mathies, R. A., in *Biological Applications of Raman Spectroscopy* (ed. Spiro, T. G.), John Wiley and Sons, New York, 1987, vol. 2, p. 1.
16. Zink, J. I. and Shin, K.-S. K., in *Advances in Photochemistry*, John Wiley and Sons, New York, 1991, vol. 16, p. 119.
17. Albrecht, A. C. and Hutley, M. C., *J. Chem. Phys.*, 1971, **55**, 4438.
18. Albrecht, A. C., *J. Chem. Phys.*, 1961, **34**, 1476.
19. Clark, R. J. H. and Dines, T. J., *Angew Chem. Int. Ed. Engl.*, 1986, **25**, 131.
20. Myers, A. B., Harris, R. A. and Mathies, R. A., *J. Chem. Phys.*, 1983, **79**, 603.
21. Grundherr, C. V. and Stockburger, M., *Chem. Phys. Lett.*, 1973, **22**, 253.
22. Stallard, B. R., Champion, P. M., Callis, P. R. and Albrecht, A. C., *J. Chem. Phys.*, 1986, **84**, 633.
23. Myers, A. B., Trulson, M. O., Pardoen, J. A., Heeremans, C., Lugtenburg, J. and Mathies, R. A., *J. Chem. Phys.*, 1986, **84**, 633.
24. Myers, A. B., Trulson, M. O. and Mathies, R. A., *J. Chem. Phys.*, 1985, **83**, 5000.
25. Dudik, J. M., Johnson, C. R. and Asher, S. A., *J. Chem. Phys.*, 1985, **82**, 1732.
26. Biswas, N. and Umapathy, S., *Appl. Spectrosc.*, 1998, in press.
27. Okamoto, H., Hamaguchi, H. and Tasumi, M., *Chem. Phys. Lett.*, 1986, **130**, 185.
28. Wootton, J. L. and Zink, J. I., *J. Am. Chem. Soc.*, 1997, **119**, 1895.
29. Kramers, H. A. and Heisenberg, W., *Z. Phys.*, 1925, **31**, 681.
30. Dirac, P. A. M., *Proc. R. Soc. London*, 1927, **114**, 710.
31. Lee, S.-Y. and Heller, E. J., *J. Chem. Phys.*, 1979, **71**, 4777; Kulander, K. C. and Heller, E. J., *J. Chem. Phys.*, 1978, **69**, 2439; Myers, A. B., Mathies, R. A., Tannor, D. J. and Heller, E. J., *J. Chem. Phys.*, 1982, **77**, 3857; Tannor, D. J. and Heller, E. J., *J. Chem. Phys.*, 1982, **77**, 202; Heller, E. J.,Sundberg, R. L. and Tannor, D. J., *J. Phys. Chem.*, 1982, **86**, 1822.
32. Feit, M. D., Fleck, Jr. J. A., and Steiger, A., *J. Comput. Phys.*, 1982, **47**, 412.
33. Kosloff, R., *J. Phys. Chem.*, 1988, **92**, 2087; Williams, S. O. and Imre, D. G., *J. Phys. Chem.*, 1988, **92**, 3363.
34. Schick, G. A. and Bocian, D. F., *J. Raman Spectrosc.*, 1981, **11**, 27.
35. Nafie, L. A., Pastor, R. W., Dabrowiak, J. C. and Woodruff, W. H., *J. Am. Chem. Soc.*, 1976, **98**, 8007.
36. Fodor, S. P. A., Copeland, R. A., Grygon, C. A. and Spiro, T. G., *J. Am. Chem. Soc.*, 1989, **111**, 5509; Bosworth, Y. M. and Clark, R. J. H., *J. Chem. Soc. Dalton Trans.*, 1974, 1749; Bosworth, Y. M., Clark, R. J. H. and Turtle, P. C., *J. Chem. Soc. Dalton Trans.*, 1975, 2027.
37. Stein, P., Miskowski, V., Woodruff, W. H., Griffin, J. P., Werner, K. G., Gaber, B. P. and Spiro, T. G., *J. Chem. Phys.*, 1976, **64**, 2159; Johnson, B. B. and Peticolas, W. L., *Ann. Rev. Phys. Chem.*, 1976, **27**, 465; Spiro, T. G. and Stein, P., *Annu. Rev. Phys. Chem.*, 1977, **28**, 501.
38. Zgierski, M. Z., *J. Raman Spectrosc.*, 1977, **6**, 53; 1976, **5**, 181.
39. Korenowski, G. M., Ziegler, L. D. and Albrecht, A. C., *J. Chem. Phys.*, 1978, **68**, 1248.
40. Asher, S. A. and Johnson, C. R., *J. Phys. Chem.*, 1985, **89**, 1375.
41. Hildebrandt, P., Tsuboi, M. and Spiro, T. G., *J. Phys. Chem.*, 1990, **94**, 2274.
42. Siebrand, W. and Zgierski, M. Z., *J. Chem. Phys.*, 1979, **71**, 3561.
43. Rimai, L., Heyde, M. E., Heller, H. C. and Gill, D., *Chem. Phys. Lett.*, 1971, **10**, 207; Friedman, J. and Hochstrasser, R. M., *Chem. Phys. Lett.*, 1975, **32**, 414.
44. Shin, K.-S. K. and Zink, J. I., *J. Am. Chem. Soc.*, 1990, **112**, 7148.
45. Reber, C. and Zink, J. I., *J. Phys. Chem.*, 1992, **96**, 571.
46. Sztainbuch, I. W. and Leroi, G. E., *J. Chem. Phys.*, 1990, **93**, 4642.
47. Phillips, D. L. and Myers, A. B., *J. Chem. Phys.*, 1991, **95**, 226; Markel, F. and Myers, A. B., *J. Chem. Phys.*, 1993, **98**, 21.
48. Trulson, M. O. and Mathies, R. A., *J. Chem. Phys.*, 1986, **84**, 2068.

49. Li, B., Johnson, A. E., Mukamel, S. and Myers, A. B., *J. Am. Chem. Soc.*, 1994, **116**, 11039.
50. Sue, J., Yan, Y. J. and Mukamel, S., *J. Chem. Phys.*, 1986, **85**, 462.
51. Markel, F. and Myers, A. B., *J. Chem. Phys.*, 1993, **98**, 21; Imre, D. G., Kinsey, J. L., Sinha, A. and Krenos, J., *J. Phys. Chem.*, 1984, **88**, 3956; Galica, G. E., Johnson, B. R., Kinsey, J. L. and Hale, M. O., *J. Phys. Chem.*, 1991, **95**, 7994; Lao, K. Q., Person, M. D., Xayariboun, P. and Butler, L. J., *J. Chem. Phys.*, 1990, **92**, 823.
52. Xu, J., Schwentner, N. and Chergui, M., *J. Chem. Phys.*, 1994, **101**, 7381; Xu, J., Schwentner, N., Hennig, S. and Chergui, M., *J. Chim. Phys.*, 1995, **92**, 541; Sension, R. J. and Strauss, H. L., *J. Chem. Phys.*, 1986, **85**, 3791.
53. Lao, K. Q., Jensen, E., Kash, P. W. and Butler, L. J., *J. Chem. Phys.*, 1990, **93**, 3958; Phillips, D. L. and Myers, A. B., *J. Phys. Chem.*, 1991, **95**, 7164.
54. Phillips, D. L., Lawrence, B. A. and Valentini, J. J., *J. Phys. Chem.*, 1991, **95**, 7570.
55. Phillips, D. L., Lawrence, B. A. and Valentini, J. J., *J. Phys. Chem.*, 1991, **95**, 9085; Phillips, D. L., Valentini, J. J. and Myers, A. B., *J. Phys. Chem.*, 1992, **96**, 2039.
56. Kwok, W. M. and Phillips, D. L., *Chem. Phys. Lett.*, 1995, **235**, 260; Phillips, D. L. and Kwok, W. M., *Chem. Phys. Lett.*, 1995, **241**, 267; Man, S.-Q., Kwok, W. M. and Phillips, D. L., *J. Phys. Chem.*, 1995, **99**, 15705.
57. Zhang, J. and Imre, D. G., *J. Chem. Phys.*, 1988, **89**, 309.
58. Johnson, A. E. and Myers, A. B., *J. Chem. Phys.*, 1995, **102**, 3519.
59. Kwok, W. M., Ng, P. K., He, G. Z. and Phillips, D. L., *Mol. Phys.*, 1997, **90**,127.
60. Myers, A. B. and Mathies, R. A., *J. Chem. Phys.*, 1984, **81**, 1552.
61. Sension, R. J., Repinec, S. T., Szarka, A. Z. and Hochstrasser, R. M., *J. Chem. Phys.*, 1993, **98**, 6291.
62. Monti, S., Orlandi, G. and Palmieri, P., *Chem. Phys.*, 1982, **71**, 87.
63. Rau, H., *Photochromism. Molecules and Systems* (eds Durr, H. and Bouas-Laurent, H.), Elsevier, Amsterdam, 1990, p. 165.
64. Rau, H. and Luddecke, E., *J. Am. Chem. Soc.*, 1982, **104**, 1616; Rau, H., *J. Photochem.*, 1984, **26**, 221; Rau, H. and Yu-Quan, S. J., *J. Photochem. Photobiol.*, 1988, **42**, 321.
65. Lunak Jr., S., Nepras, M., Hrdina, R. and Mustroph, H., *Chem. Phys.*, 1994, **184**, 255.
66. Dyck, R. H. and McClure, D. S., *J. Chem. Phys.*, 1962, **36**, 2326.
67. Biswas, N. and Umapathy, S., *J. Phys. Chem.*, 1997, **A101**, 5555.
68. Lawless, M. K., Wickham, S. D. and Mathies, R. A., *J. Am. Chem. Soc.*, 1994, **116**, 1593; Lawless, M. K., Wickham, S. D. and Mathies, R. A., *Acc. Chem. Res.*, 1995, **28**, 493; Reid, P. J., Shreve, A. P. and Mathies, R. A., *J. Phys. Chem.*, 1993, **97**, 12691.
69. Chakrabarti, N., Kalyanaraman, C. and Sathyamurthy, N., *Chem. Phys. Lett.*, 1997, **267**, 31.
70. Marconi, G. and Houben, J., *J. Chem. Soc. Faraday Trans. 2*, 1985, **81**, 975.
71. Jimenez, R., Fleming, G. R., Kumar, P. V. and Maroncelli, M., *Nature*, 1994, **369**, 471.
72. Rosenthal, S. J., Xie, X., Du, M. and Fleming, G. R., *J. Chem. Phys.*, 1991, **95**, 4715.
73. Maroncelli, M., *J. Chem. Phys.*, 1991, **94**, 2084.
74. Neria, N. and Nitzan, A., *J. Chem. Phys.*, 1992, **96**, 5433.
75. Roy, S. and Bagchi, B., *J. Chem. Phys.*, 1993, **99**, 1310, 9938.
76. Doorn, S. K., Blackbourn, R. L., Johnson, C. S. and Hupp, J. T., *Electrochim. Acta*, 1991, **36**, 1775.
77. Ci, X. and Myers, A. B., *J. Chem. Phys.*, 1992, **96**, 6433.
78. Markel, F., Ferris, N. S., Gould, I. R. and Myers, A. B., *J. Am. Chem. Soc.*, 1992, **114**, 6208.
79. Myers, A. B., *Chem. Phys.*, 1994, **180**, 215; Myers, A. B. and Li, B., *J. Chem. Phys.*, 1990, **92**, 3310.
80. Kulinowski, K., Gould, I. R., Ferris, N. S. and Myers, A. B., *J. Phys. Chem.*, 1995, **99**, 9017, 17715.
81. Ci, X., Pereira, M. A. and Myers, A.B., *J. Chem. Phys.*, 1990, **92**, 4708.
82. Myers, A. B., Li, B. and Ci, X., *J. Chem. Phys.*, 1988, **89**, 1876.
83. Myers, A. B., *Chem. Rev.*, 1996, **96**, 911; *J. Raman Spectrosc.*, 1997, **28**, 389; *Acc. Chem. Res.*, 1997, **30**, 519.
84. Kwok, W. M., Phillips, D. L., Yeung, P. K.-Y. and Yam, V. W.-W., *J. Phys. Chem.*, 1997, **101**, 9286; *Chem. Phys. Lett.*, 1996, **262**, 699.
85. Barbara, P. F., Meyer, T. J. and Ratner, M. A., *J. Phys. Chem.* 1996, **100**, 13148.
86. Williams, R. D., Petrov, V. I., Lu, H. P. and Hupp, J. T., *J. Phys. Chem.*, 1997, **A101**, 8070.
87. Doorn, S. K. and Hupp, J. T., *J. Am. Chem. Soc.*, 1989, **111**, 4704.
88. Blackbourn, R. L., Johnson, C. S., Hupp, J. T., Bryant, M. A., Sobocinski, R. L. and Pemberton, J. E., *J. Phys. Chem.*, 1991, **95**, 10535.

ACKNOWLEDGEMENTS. We thank the Council of Scientific and Industrial Research, the National Laser Programme of the Department of Science and Technology and Jawaharlal Nehru Centre for Advanced Scientific Research, Government of India for financial assistance and the Supercomputer Education and Research Centre of Indian Institute of Science for providing the computing facilities necessary to carry out the present work.